Journal of Energy Storage 32 (2020) 101726

Contents lists available at ScienceDirect

Journal of Energy Storage

journal homepage: www.elsevier.com/locate/est

Experimental study of the effect of inclination angle on the paraffin melting process in a square cavity

Abdel Illah Nabil Korti*, Hocine Guellil

ETAP Laboratory, University of Tlemcen, 230, 13000

ARTICLE INFO

Keywords:
Thermal Storage
Latent heat
PCM
Paraffin
Natural convection

ABSTRACT

The transient melting process of a phase change material (PCM) is strongly affected by its inclination angle caused by the behavior of buoyancy-driven natural convection. An experimental study is carried out to investigate the effect of this inclination on the thermal behavior during PCM melting contained in a square cavity. The range of inclination angle from 0° (vertical), 45° (inclined) and 90° (bottom) is considered. Paraffin with a melting range of 49-54°C is used as PCM. The volumetric shrinkage of PCM during solidification preceding the melting experiments leads to the development of a large void in the free surface PCM-air. The effects of inclination and shrinkage phenomenon are analyzed by visualizing the solid-liquid interface and measuring temperatures by thermocouples and infrared camera. Results show that the inclination angle has a great influence on the natural convection behavior, and affects the melting front progression and the heat transfer rate. The total melting time for the bottom and inclined cavities cases were, on average, 56% and 48% less than the vertical one, respectively. The volumetric shrinkage disrupts significantly the melting process in the vertical and inclined cases. The natural convection is more intense in the bottom case and the global average Nusselt number increases during the strong convection by about 10% and 21% compared to the inclined and vertical cases, respectively.

1. Introduction

Thermal energy storage (TES) systems based on the use of PCM are implemented in different engineering fields: solar heating, hot water, cooling technology for electric device, air conditioning, building structures insulation, etc. Good understanding of heat transfer during melting process is essential for predicting the storage system performance with accuracy and avoiding costly system overdesign. Using PCM in the TES has become a key area of research during the three past decades. Large amounts of heat can be stored or released during the phase change process of PCM. An enormous amount of experimental, numerical, and modeling work has been carried out to understand the heat transfer behavior of these materials. The dominant heat transfer mechanisms during the melting process are heat conduction and convection. Since most PCMs have a low thermal conductivity, many efforts have been devoted to improving both thermal conductivity and heat transfer of the latent heat thermal energy storage LHTES system. The most common methods used are incorporating high thermal conductivity additives into PCMs or embedding PCMs into a matrix. Improving the natural convection heat transfer in the liquid PCMs is another way to enhance the heat transfer of PCMs [1,2]. Guellil et al. [3] studied experimentally the performance of a novel LHTES unit using a finned U-tubes exchanger filled with paraffin. The study observed that using the fins improves the energy stored more than five times. Increasing the power supply by 32% decreases the average melting interval by 34% and delays the time of solidification starting by about 30%. Korti et al. [4] presented an experimental study of the charging and discharging process of the cylindrical LHTES filled by three types of paraffin. They concluded that adding the oil of engine to the paraffin accelerates the charging and discharging heat process by 42.4% and 66 %, respectively. Bondareva [5] analyzed the influence of the physical properties of PCMs and the concentration of nanoparticles on heat and mass transfer inside a closed radiator with fins exposed to a constant volumetric heat generation. The results showed that n-octadecane, lauric acid, and RT-80 are the most effective for cooling at high heat generations. An increase in the mass fraction of particles from 2% to 6% leads to a significant weakening of the convective circulation of the melt and can lead to a decrease in the critical operating time. Tiari [6] was studied numerically the startup process of a high temperature LHTES system assisted by finned heat pipes with different configurations of embedded heat pipes. Increasing the quantity of heat pipes reduces the thermal resistance between heated surfaces and the PCM

* Corresponding author.
E-mail addresses: korti72@yahoo.fr (A.I.N. Korti), guellil10@yahoo.fr (H. Guellil).

https://doi.org/10.1016/j.est.2020.101726
Received 1 April 2020; Received in revised form 24 July 2020; Accepted 27 July 2020
Available online 11 August 2020

Nomenclature

A	surface area (m^2)
C	specific heat capacity (kJ/kgK)
f_l	liquid fraction
g	acceleration of gravity (m/s^2)
h	heat transfer coefficient (W/m^2K)
H	height (m)
K	thermal conductivity (W/mK)
L_f	latent heat of fusion (kJ/kg)
M	mass (kg)
Nu	Nusselt number
Q_{st}	thermal energy stored (kJ)
Ra	Rayleigh number
Ste	Stefan number
T	temperature (°C)
t	time (s)
W	Width (m)
V	volume (m^3)

Greek symbols

α	thermal diffusivity (m^2/s)
θ	inclination angle (°)
ρ	density (kg/m3)
β	coefficient of volumetric thermal expansion ((K^{-1})
ν	kinematic viscosity (m^2/s)

Subscripts

0	total
ins	insulation (Rockwool)
l	liquid
m	melting temperature
s	solid
w	hot wall

melt front, resulting faster charging process and lower container base wall temperature. The natural convection in the melting process significantly increases the melting rate and reduces the container base wall temperature

After the selection of the PCM type, the geometry of the PCM container is the most influential factor on the thermal performance of PCM systems. Some studies have been concerned to the heat transfer in square cavities heated from the side [7]. The melting of RT44HC has been explored experimentally in a rectangular cavity heated from both the left and right sides [8]. The study shows that increasing the input power from 675 to (960 W/m^2 and 1295 W/m^2) reduces the total time for the melting process by 27% and 43 %, respectively. Conduction is the dominant mode of heat transfer during the early stage of melting which is followed by a short transition period before convection dominates the remainder of the melting process. However, the configuration of a PCM within a rectangular container heated from bottom has received comparably less attention. This configuration is important to dissipate heat from electronic devices. Madruga et al. [9] studied numerically the melting dynamics of n-octadecane within square geometries with periodic boundary conditions along the horizontal direction heated from below with different sizes. They have identified four different regimes over time: conduction, linear, coarsening and turbulent regimes. The first two regimes appear at all domain sizes. However, the third and fourth regimes require a long advance of the solid/liquid interface (greater than 3.5 cm). Finally, the turbulent regime leads to a very irregular solid/liquid interface with strong fluctuations of the amplitude (Rayleigh-Benard instability).

The thermal behavior during the melting of PCM is strongly affected by the nature of natural convection in the liquid phase, and therefore the orientation of the strength of buoyancy. Few investigators have studied the influence of the inclination angle on the PCM melting process in the enclosure. Among the researchers who have treated this problem numerically, Ye [10] studied the influences of inclination angles (from 0 to 360°) of the quadrantal cavity on the thermal performance of TES system. It is found that the inclination angles affects dramatically the time of complete thermal energy storage and convection currents. The best performance is obtained for an inclination angle of 225° and for the bottom heating from the curved wall. Zennouhi [11] presented a two-dimensional numerical simulation of the melting process of Galium (PCM with melting temperature of 29.78°C) in a rectangular enclosure for different inclination angles. Increasing the inclination angle from vertical to bottom produces irregular liquid-solid interface and increases the strength of the vertical flow structures in the liquid region. The shapes of the liquid-solid interfaces during the melting process in the bottom case show the generation of Benard convection cells in the liquid region. It is also found that the rate of the melting increases by increasing the inclination from vertical to bottom one. Hong [12] simulated numerically the LHTES in a two-dimensional rectangular cavity with partially thermally active parts for different inclination angles. The best thermal behavior can be reached with the bottom case whereas the bad one is formed when the hot wall is vertical. With the best case, the request time to reach complete melting and the maximum stored energy of 75 kJ is reduced by 42.2% and 46.9%, respectively. Bondareva [13] performed numerically the heat transfer inside a closed rectangular cavity contained a paraffin with nanoparticles and heated from copper profile with finning. The simulation has been carried out for different inclination angles (0° vertical, 90° bottom and 180° top). The most intense melting is observed for the bottom case. The addition of nanoparticles to the paraffin decreases the time for complete melting for all the considered cavity inclination angles.

Among the experimental investigators, Kamkari [14] studied the dynamic thermal behavior of PCM (Lauric acid with range of melting 43.5-48.2°C) melting in a rectangular enclosure at various inclination angles (vertical, bottom and 45° inclination). The enclosure is heated isothermally from one side while the other walls are thermally insulated. For the same hot wall temperatures, the total melting time for the inclined and bottom cases were, on average, 35% and 53% less than the vertical case, respectively. The time-averaged Nusselt number showed 11% and 35% enhancements when the wall temperature was increased from 55 to 60 and 70°C, respectively. Bouadila [15] studied experimentally the inclination effect of a storage system using paraffin filled in cavity integrated behind the absorber solar water heater. For increasing the inclinations from 0 (vertical) to 30, 45 and 60°, the non uniformities in the interface shape are more pronounced which can be attributed to an intensification of the flow in the liquid phase. Inclination of the cavity has a significant effect on the interface progression only when the process is dominated by natural convection and at advanced stages of the phase change process. Joneidi [16] investigated the effect of heat flux and inclination angle variation in a rectangular PCM (RT35 melting range 29-35°C) containing cavity. At the early stages of the process, conduction becomes the dominant heat transfer mechanism and convection appears when melt becomes available. The increases in the angle from 0° to (45° and 90°), increases melting time (55 and 95 %), the average temperature of the PCM and the final stored energy. An experimental study is carried out by Avci [17] to investigate the effect of inclination angle (from vertical to bottom) on the thermal performance of a rectangular cavity filled by N-eicosane (melting range of 35-37°C). The study concluded that the velocity of the liquid-solid interface increases with an increase in the

inclination angle due to the domination of convective cells. The melt fraction increases with an increase in the inclination angle. Yang [18] studied the melting behaviors of paraffin embedded in open-cell metal foams (composite-PCM) at different inclination angles. Compared with the 0° (vertical) case, the full melting time is reduced by 12.28%, 22.81%, and 34.21% at 30°, 60°, and 90° (bottom), respectively. However, little influence (maximum is 4.35%) is found in full melting time in composite-PCM under inclined situations. Natural convection significantly affects heat transfer in pure PCM but contributes little to composite-PCM for an inclined configuration. Experiments are performed by Allen [19] to analyze the impact of system inclination (ranging from 0° to 90°) on the melting and solidification of a phase change material (PCM) in a cylindrical enclosure. A total of 6 configurations and 28 case studies were investigated with varying orientation and driving temperatures. Orientation has minimal effect on the solidification process due to conduction dominated heat transfer. The heat pipe-foil-PCM configuration with porosity of 0.945 and driving temperature of 17°C was capable to increasing the melting rates by about 9 times and reducing the total solidification and melting times to about 3% and 12%.

The above cited experimental literature revealed that the authors are more interested by the rectangular cavities. The results show a large difference in quantifying the acceleration of the melting rate with increasing the inclination angles. To our knowledge, no experimental study has been carried out on the effect of inclination angle on the paraffin melting process contained in a square cavity. In addition, the volumetric shrinkage of paraffin during solidification that precedes the melting experiences leads to the development of a large void in the upper part of the PCM with irregular free surface PCM-air. This study presents the detailed experimental analysis of the thermal behavior of pure paraffin with three angles 0°, 45°, and 90°. We tries to show the effect of the shrinkage phenomenon on the melting process in the different inclinations. The present study aims to provide benchmark with experimental reference and different correlations for the practical applications of LHTES system with different inclinations.

2. Experimental procedure

2.1. Geometric details

An experimental apparatus has been designed and built to visualize the instantaneous solid–liquid interface progression, and accurately measure temperature distribution within the PCM. The cavity is made from 20 mm thick glass (thermal conductivity of 0.17 W/m K) to allow observation of the melt fraction development during the experiment. The container was a square enclosure with inside dimension of 45 mm in width, 120 mm in height and 120 mm in depth. The right wall of the cavity is made in the form of a small copper cavity to contain a regulated electrical heater to provide a constant heat flux. Except the front side, All the faces are insulated using Rockwool with thickness of 72 mm (thermal conductivity of 0.04 W/m K), Fig. 1.a.

2.2. Experimental apparatus

The back side of cavity has been pierced to pass 9 K-type thermocouples in the PCM interior zone, and record the temperature evolution of the PCM. 1 K-type thermocouple is employed for the heating surface temperature and the last one senses for the ambient temperature. Fig. 2 displays the location of the thermocouples whose probe senses the temperatures of the mid plane parallel to *x-y* plane. All the thermocouples are connected to PC computer via a data logger (NI c-DAQ 9174) using a thermal modules (NI 9211) to record temperatures during the melting process. An infrared camera (Testo i875) with a resolution of 320 × 240 Pixels was mounted in the front of the cavity test to record a thermal field of the paraffin during melting. The temperature measurement with thermocouples can be used to adjust the infrared measurements. In order to see the effect of the cavity orientation on the behavior of the natural convection flow during paraffin melting, three configurations are used: vertical heating by right, bottom heating, and 45° inclined heating (Fig. 2). The thermal physical properties of the PCM used are shown in Table 1.

The PCM (paraffin wax CAS 8002-74-2) was initially melted on the fire and poured into the test cavity. After, the cavity was maintained at room temperature for 24 h to ensure that the solid paraffin obtained was almost the same physical state before each experiment. Thus, it was observed the creation of a concave shape on the free surface of the PCM at the end of each solidification. This phenomenon is mainly caused by the volumetric shrinkage of paraffin during solidification. It will directly influence the evolution of front melting at the top of PCM, Fig. 1.b. Three sets of experiments were conducted for each inclination angles. At the beginning of the experiment, the whole cavity and the material are in thermal equilibrium with the ambient temperature (23.5°C). The moment that the heater turns on is the same as the data acquisition and photo capturing initiation. The value of the heat flux applied at the hot wall is about 15 W (2700 W/m^2). The data records take place every 2 s while the photos are taken each 5 min. The liquid fraction is estimated via photography. Fig. 3 illustrates the time evolution of the hot wall temperature. After the initial transition, it can be seen that the hot wall temperature reaches a constant value of 97.5 ± 3°C, 95.5 ± 2°C and 91 ± 1.5°C respectively in the vertical, bottom and inclined cases. Thus, we think that the buoyancy force favors the evacuation of heat from the hot wall in the bottom case causing the decrease of its temperature. In the steady stage, the average temperature of the hot wall imposed is about 94.7°C. The time of this transition is about 40 min in the vertical case and 68 min in the bottom and inclined cases.

2.3. Uncertainty analysis

The uncertainty of experimental results is often affected by the inevitable errors in experimental measurement, and depends on the uncertainty of measuring instruments. The maximum uncertainty in temperature measurement is equal to ± 0.5°C

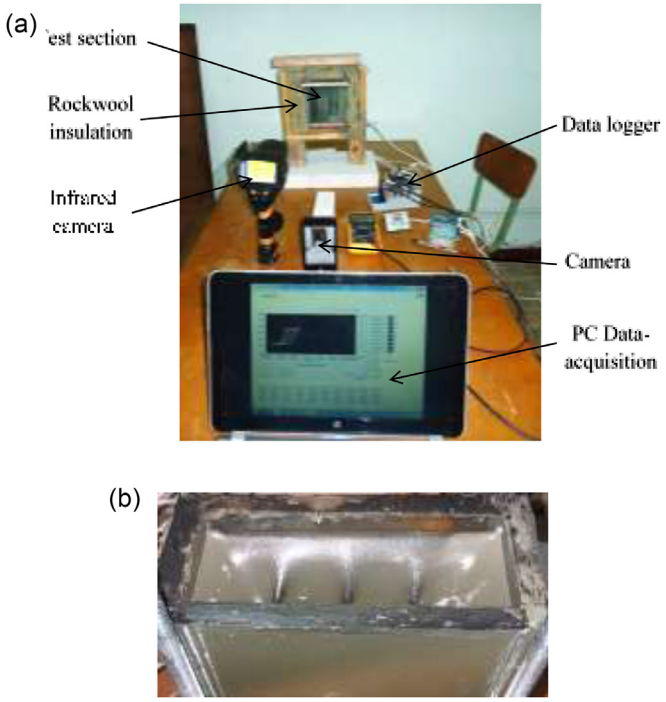

Fig. 1. a. Picture of the laboratory setup. **b.** Picture of the concave form at the free surface of paraffin.

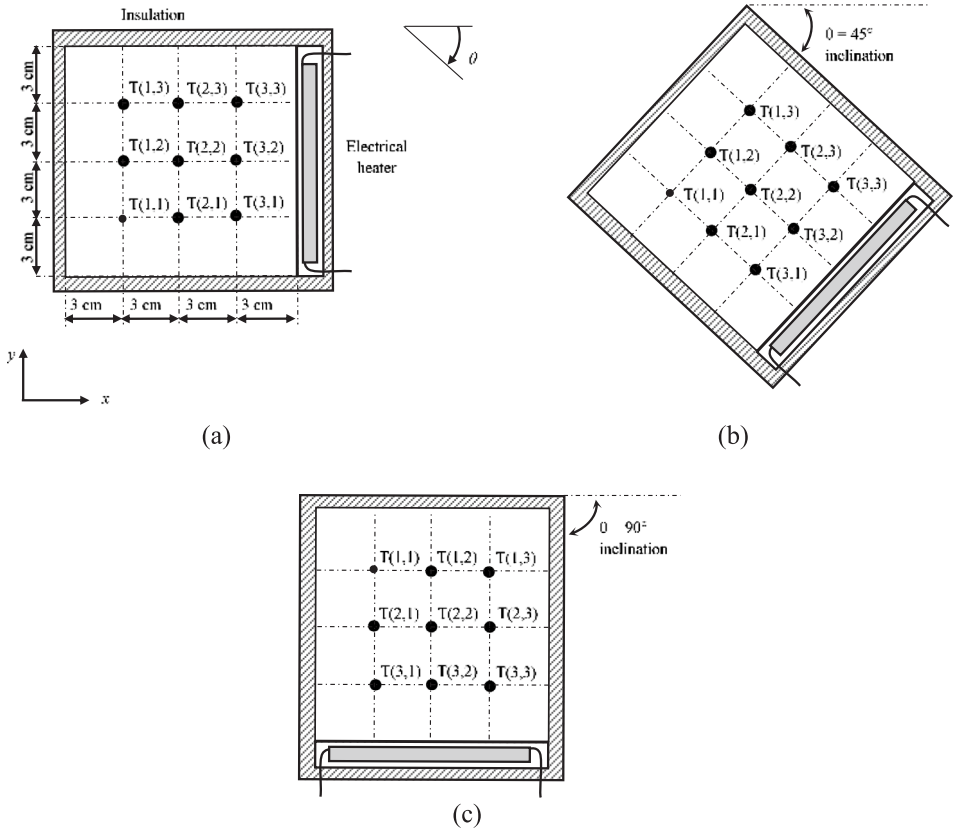

Fig. 2. Schematic diagram of the experimental procedure (a) vertical, (b) inclined and (c) bottom heating.

Table 1
Thermal physical properties of paraffin used [20,21].

Properties	Typical values
Melting temperature (°C)	49-54
Latent heat (kJ/kg)	176
Specific heat (liquid) (kJ/kg-K)	2.9
Specific heat (solid) (kJ/kg-K)	2.7
Thermal conductivity (liquid) (W/m-K)	0.12
Thermal conductivity (solid) (W/m-K)	0.21
Density (liquid 65°C) (kg/m^3)	790
Density (solid 24°C) (kg/m^3)	916
Dynamic viscosityd(kg/m-s)	0.0036
Coefficient of thermal expansion (K^{-1})	9.1 × 10^{-4}

In the experiments, the temperatures measured by the thermocouple can offer only the temperatures at predefined locations. To obtain the temperature field during paraffin melting we can use an infrared IR camera focused on the outside front side of the PCM cavity. It is necessary to compare the values of the IR temperature with those of the thermocouples to calibrate the value of the emissivity in the camera (Fig. 4). Thus, the emissivity was taken of 0.95 when the average temperature measured is lower than 45°C and of 0.69 when is greater than 45°C. The maximal relative error recorded by the IR camera is about 24 % and the average error is about 5 %.

The PCM mass measurement error are ± 0.8 g and the maximum uncertainty of measuring the PCM mass is 1.6%.

The maximum uncertainty of measuring the total area with an image processing system with a resolution of 540 × 864 pixels is [16]

$$\frac{\Delta V_0}{V_0} = \frac{1}{540} + \frac{1}{864(H_m/W_m)} = 0.3\%$$

Since the minimum solid phase fraction measured was 3%, the maximum deviation in determining the area of the solid phase is

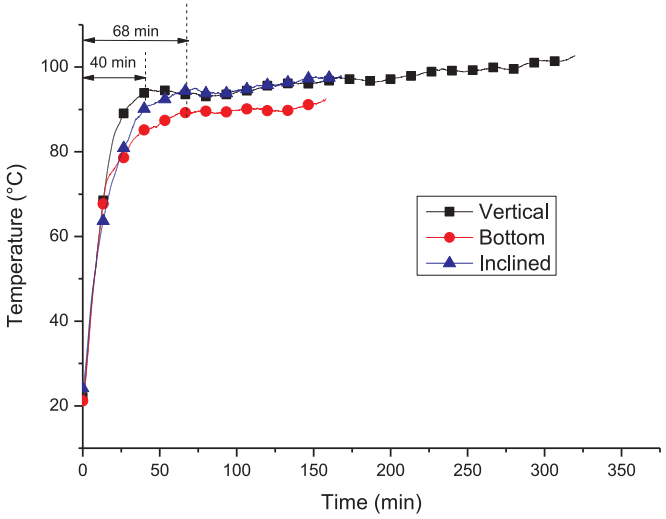

Fig. 3. Time evolution of hot wall temperature.

$$\frac{\Delta V_s}{V_s} = \frac{1}{540} + \frac{1}{864(H_m/W_m)(V_s/V_0)} = 4.16\%$$

Thus, the maximum uncertainty in determining the melt fraction from the photos is

$$\frac{\Delta V_l}{V_l} = \frac{\Delta V_s}{V_s} + \frac{\Delta V_0}{V_0} = 4.46\%$$

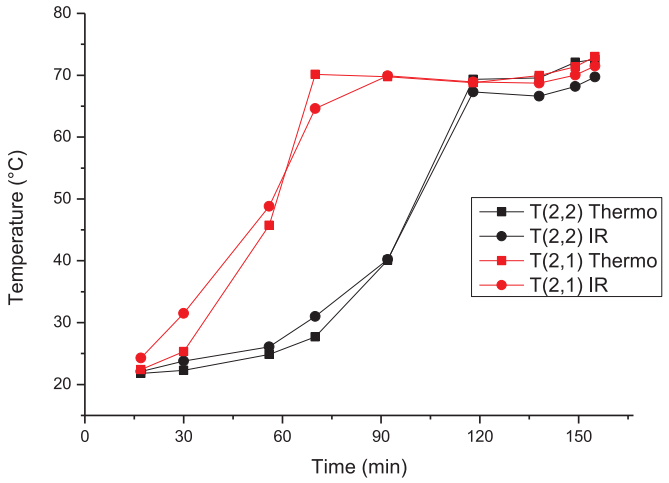

Fig. 4. The infrared and thermocouple recorded temperatures for bottom case.

3. Results and interpretations

3.1. Pattern of the solid–liquid interface

Fig. 5 shows the sequential photographs of melting front and IR temperature during the melting of paraffin heated vertically. Initially, the melting process starts from the heated wall and the solid-liquid interface is parallel to the heated wall showing that the heat transfer is dominated by conduction. After 40 min, the melting front advances to the left with a curvature registered at top. This phenomenon results in the gradually development of natural convection in the liquid paraffin. The temperature differences in the liquid (49-81°C) are sufficient to produce anticlockwise convection currents. As time elapses, temperatures increases and the density of the liquid PCM adjacent to the hot wall decreases, and the liquid PCM adjacent to the hot wall goes up by buoyancy effect. It flows horizontally before descending along the solid/liquid interface reducing in temperature. The change in direction from vertical to horizontal flow observed at the top of the cavity promotes the inclination of the temperature contours. The heat flow accelerates the melting process at the top of the thermal cavity and delays it at bottom. Then, natural convection dominates the heat transfer and the curvature of the melting front becomes important until the end of melting. In all, the IR image shows that the temperature gradient in the liquid phase is higher (until 48°C) than the solid phase (until 19°C). This shows that the intensity of heat transfer in the solid phase is lower than the liquid one due to the poor thermal conductivity of the paraffin. The results show that the mushy zone lies in a temperature range between 49 and 54°C. It observed a cap form of paraffin solid developed at the top of the melt layer until 80 min. The length of this cap can reach 2.8 cm representing around 23% of the width of cavity. This phenomenon is caused by the volumetric shrinkage of paraffin during the solidification process that precedes the experience (discussed before). Then, a large void exists in the upper part of the paraffin with irregular boundary between the PCM and air. This phenomenon, which seriously disrupts the progression of melting, is generally neglected in numerical simulation works [22]. The complete melting of the paraffin is achieved after about 5h20. In addition, the results show that paraffin melting is accompanied by a volumetric expansion around 7%.

Fig. 6 shows the sequential photographs of melting front and IR temperature during the melting of paraffin heated by bottom. In all, it observed that the solid/liquid interface is almost parallel to the bottom wall of the cavity, and the solid liquid interface of paraffin rose with time. The conduction regime dominates the heat transfer at the beginning of melting and no motion is present. The PCM is melted above the hot wall and the melting front advances vertically upwards, with the interface flat and parallel to the bottom hot wall. Once the melting front reaches a height of 1.4 cm (after 20min), the temperature differences (49-73°C) are sufficient to produce a natural convection currents and the liquid layer destabilizes due to gravity through a Rayleigh-Benard instability. The number and the size of the Benard cells are dependent on heat flux imposed and the height of the melting front. At this time, the instability creates an array of about eleven counter-rotating convective cells. As the interface progresses, the convective rolls is vertically stretched leading to larger convective cells and the number of the counter-rotating rollers decreases. At 40 min, melting front reaches a height of 3.4 cm and about seven counter-rotating convective cells is observed. At the latest (140 min), the melting front becomes more stable with the presence of a single dominant cell in the liquid phase. Like the previous case, the IR image shows that the temperature gradient in the liquid phase is higher (until 53°C) than the solid phase (around 14°C). This shows that the heat transfer in the solid phase is lower due to the poor thermal conductivity of the paraffin. In practice, it is difficult to ensure a uniform heat flux along the hot wall. This problem has caused a slight curvature on the isotherms at the left of the cavity. It observed the no presence of the cap phenomenon during the melting process. Indeed, the melting front reaches the top of the paraffin only at the end of the process. Thus, the melting progress is influenced by the volumetric shrinkage only at the end of the melting. This phenomenon can be neglected in numerical simulation works

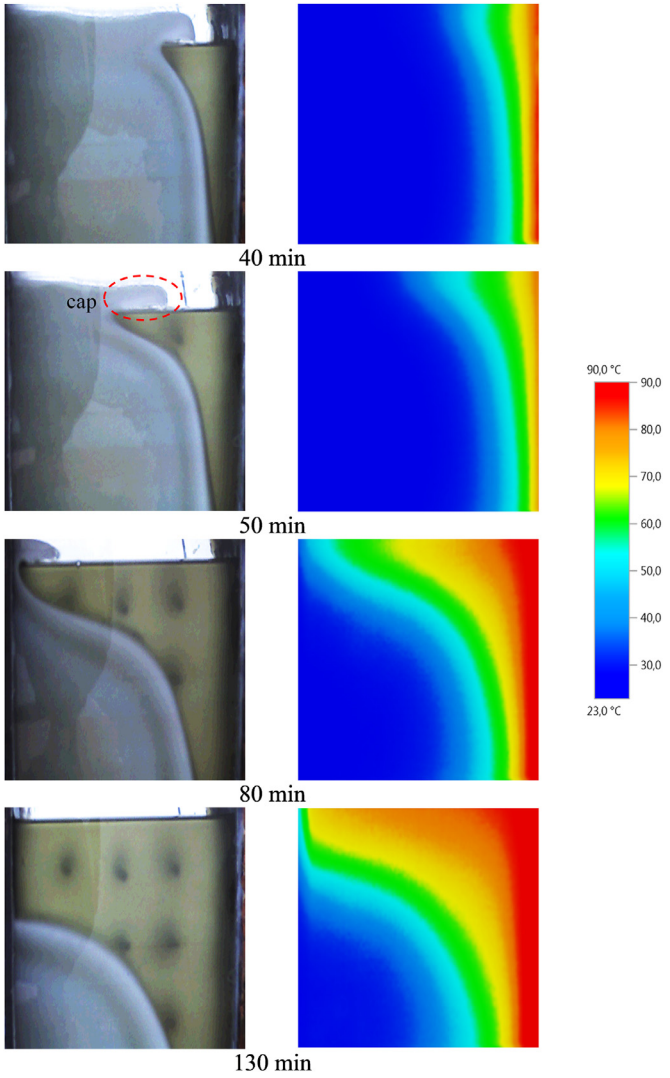

Fig. 5. Time evolution of the melting process (left) and IR image (right) of the paraffin heated vertically.

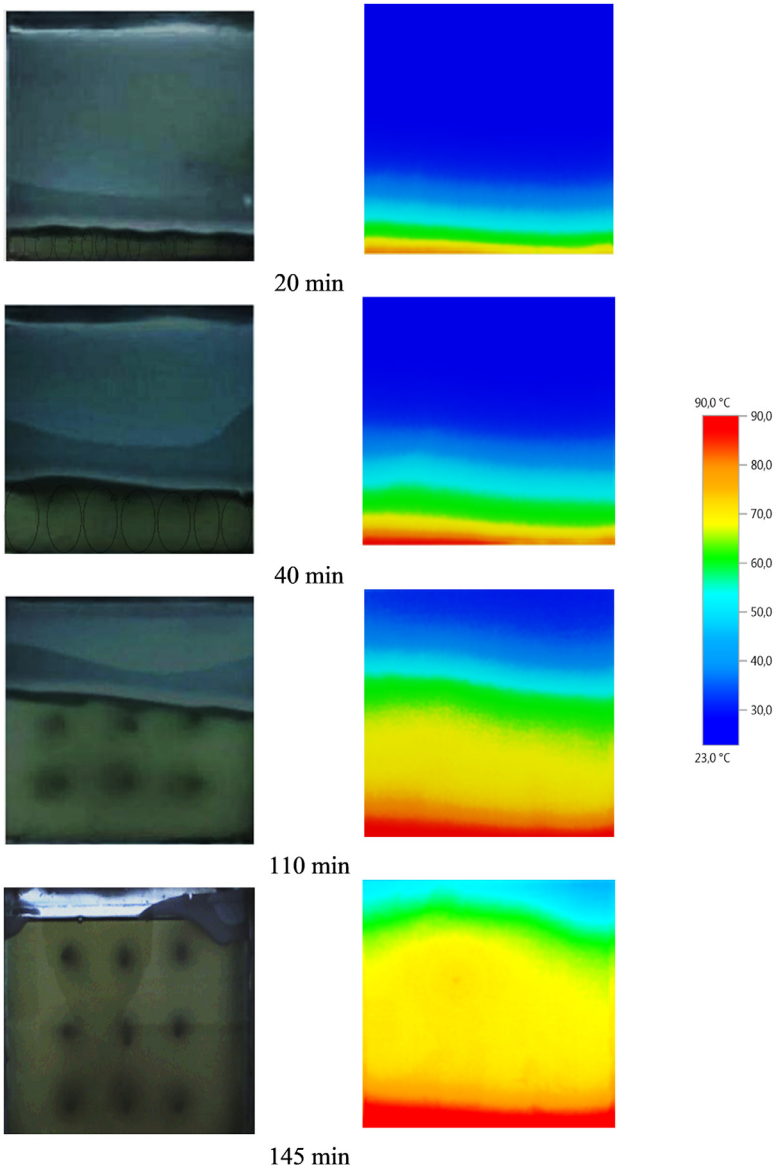

Fig. 6. Time evolution of the melting process (left) and IR image field (right) of the paraffin heated by bottom.

treating the heating by bottom. The complete melting of the paraffin is achieved after 2h20, it's represent 3 h less than the case of vertical hot wall.

Fig. 7 shows the sequential photographs of melting front and IR temperature during the melting of paraffin heated by inclined wall (45°). At the beginning, the paraffin begins to melt at the vicinity of the heated wall. There is no convection movement in the liquid phase and the solid/liquid interface is parallel to the heated wall. Heat transfer throughout the paraffin is dominated by conduction. Until 30 min, the isotherms are always stratified on the range of (49-64°C) and the convection flow starts to dominate gradually the heat transfer in the liquid phase. The instability observed at the molten front indicates the presence of Rayleigh-Benard multi cellular flow patterns. At 60 min, a small curvature is observed at the right of the melting front that shows a slight acceleration of the fusion along the upper right wall.

At 90 min, the melting front becomes curved and the Rayleigh-Benard multi cellular convection is converted to the anticlockwise convection currents at the center of the heated wall with presence of a small cell at the center at the top of paraffin. The density of the liquid PCM adjacent to the hot walls decreases and the liquid PCM adjacent to the hot wall goes up by buoyancy effect along the upper right wall. It flows horizontally along the top of liquid layer before descending along the solid/liquid interface reducing in temperature. The change in direction leads to the inclination of the temperature contours. The heat flow accelerates the melting process at the top of the liquid layer and the bottom corner. Like the case of the vertical wall heating, the volumetric shrinkage of paraffin during solidification that precedes the experience leads to the development of the cap phenomenon along the melting front (90 min).

Due to the inclination of the cavity, the upper surface of the paraffin is smaller than the two previous cases. Thus, the length of this cap can reach 4 cm representing around 55% of the top of paraffin. The complete melting of the paraffin is achieved after 2h35, 15 min after the bottom case and 2h35 before the vertical case.

3.2. Melting rate

Fig. 8 shows the comparison between the time evolutions of the paraffin liquid fraction for different inclinations, obtained experimentally and by the correlation. Overall, the melting rate increases by increasing the inclination angle. The results show that the melting process evolves through two different steps. At the beginning, the conduction

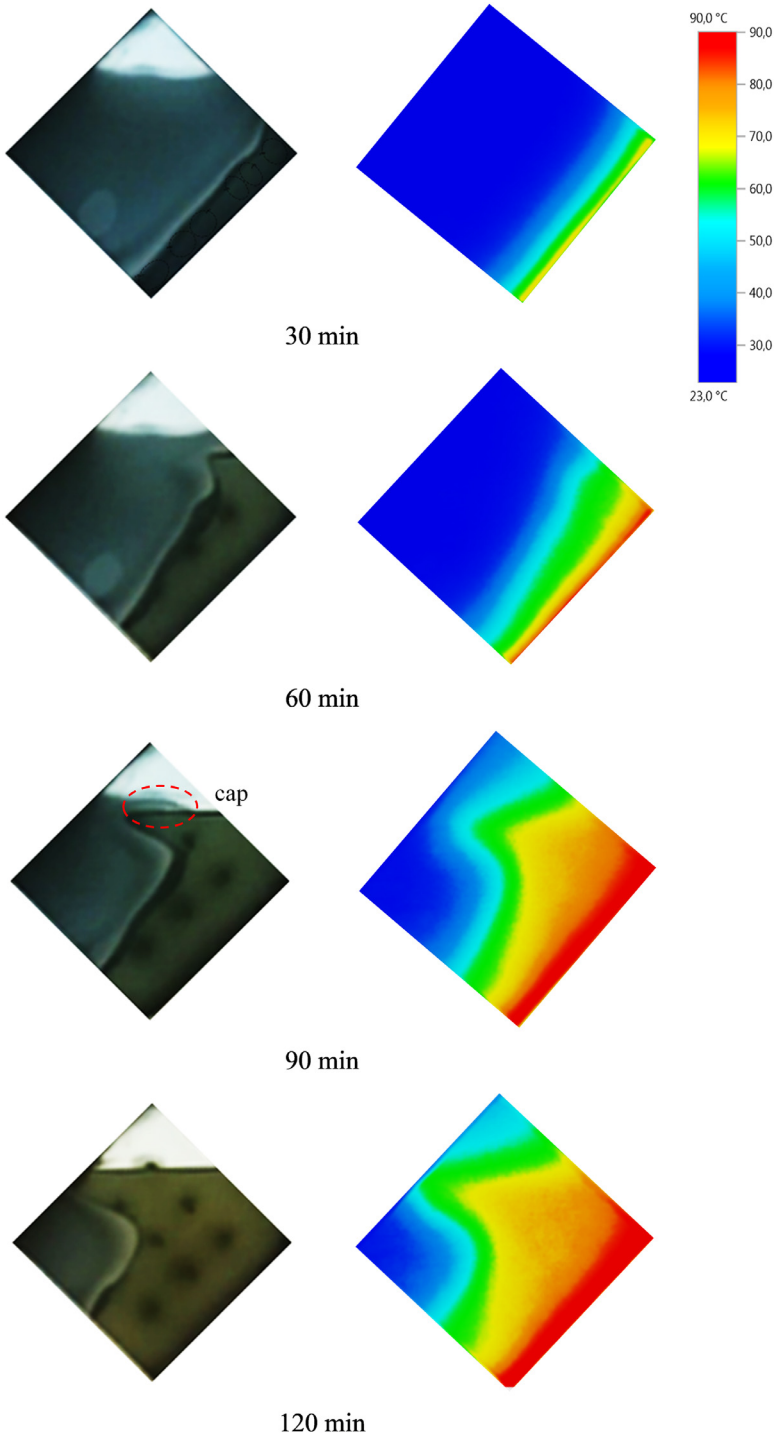

Fig. 7. Time evolution of the melting process (left) and thermal field (right) of the paraffin with an inclination heating.

dominates heat transfer and the melting rate is so identical for three different inclinations. After, the effect of convection increases and dominates gradually the heat transfer in the liquid phase. For the bottom and inclined cases, melting fraction vary almost linearly with time until the end of the melting process. Then, the heat transfer rate is not affected by the melt layer thickness during the phase change process when melting from the bottom. For the vertical case, the liquid fraction evolution deviates from a linear trend and the melting rate decreases. This may be due mainly to the different intensity of natural convection. Thus, Rayleigh-Benard multi cellular convection contributes to accelerate the melting rate in the bottom case. In the inclined case, the passage from Rayleigh-Benard multi cellular convection to the anticlockwise convection currents delays the melting rate compared to the bottom case. In the vertical case, the anticlockwise convection current developed in the liquid phase decreases the melting rate. The total melting time for the bottom and inclined cavity were, on average, 56% and 48% less than the vertical cavity, respectively. These results are closer to those obtained by Kamkari [14]. The inclination of the cavity can, depending on the case, accelerates or delays the melting speed. Therefore, it is possible to choose the inclination of the cavity to optimal improve the melting process. The liquid fraction evolution depends on the inclination angle of cavity θ (0°: vertical, 45°: inclined,

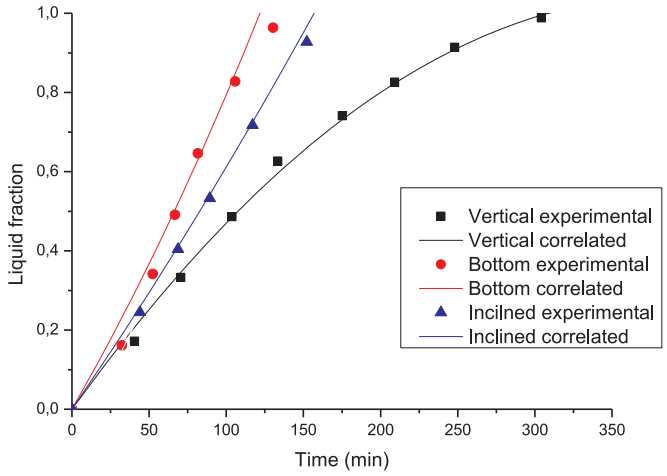

Fig. 8. Time evolution of the volume fraction of liquid (experimental and correlation).

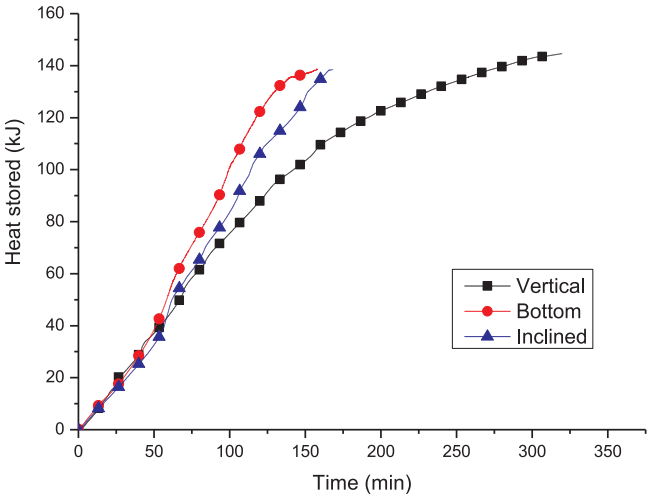

Fig. 10. Time evolution of the energy stored by PCM for different inclinations.

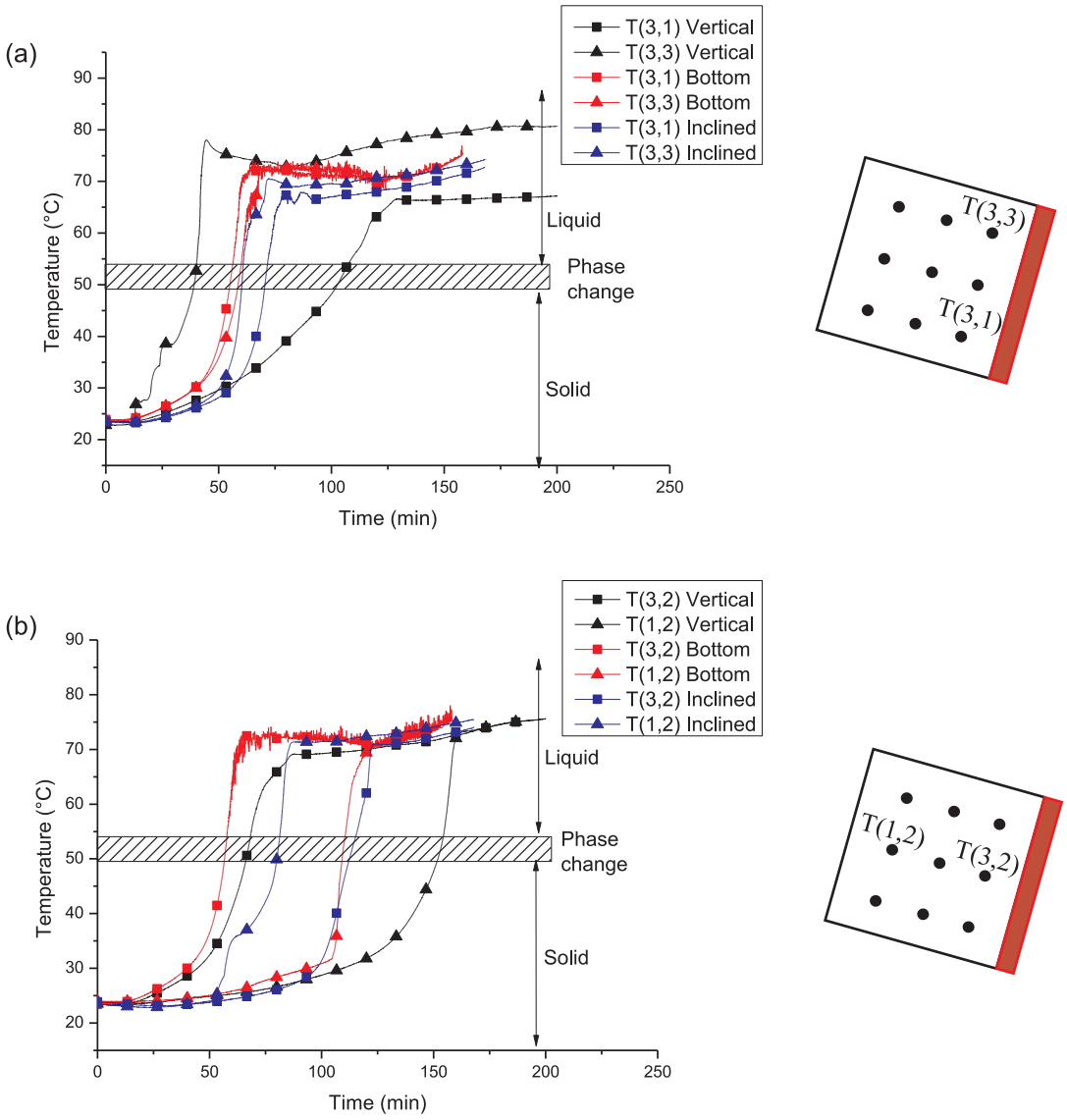

Fig. 9. a. Time evolution of the temperature along the hot wall for the three inclinations. **b**. Time evolution of the temperature along the axis of the cavity perpendicular to the hot wall.

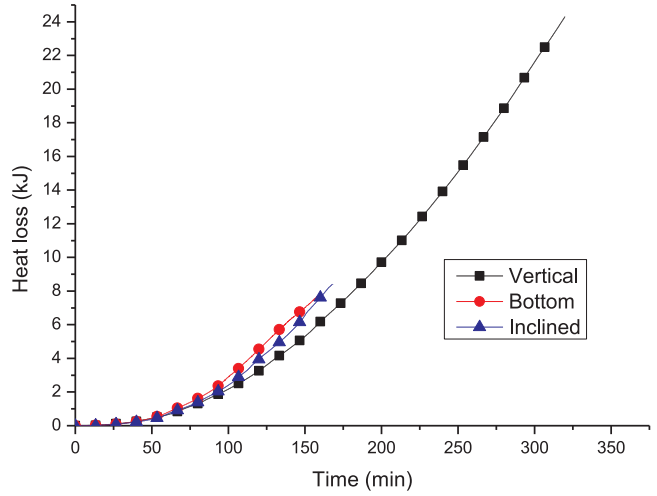

Fig. 11. Time evolution of the energy loss by cavity for different inclinations.

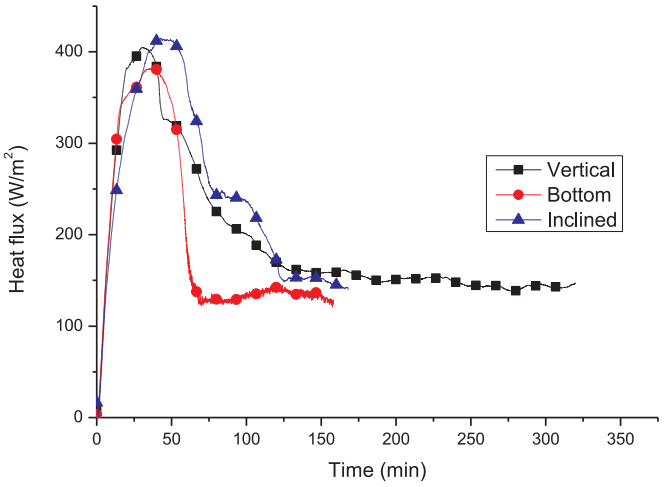

Fig. 12. Time evolution of the heat flux transferred from the hot wall for different inclinations.

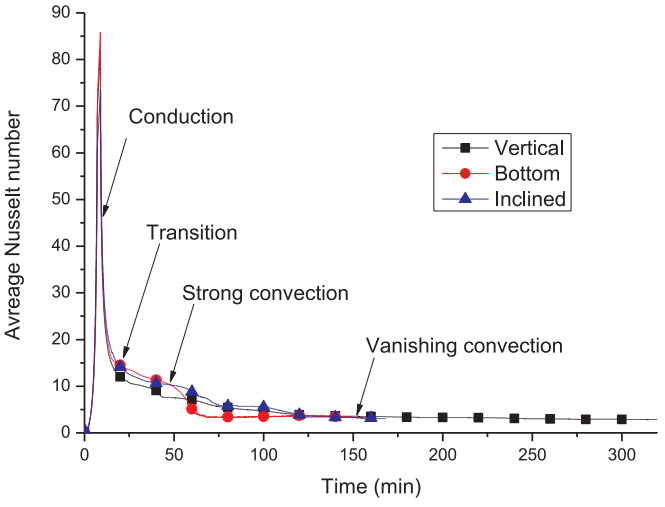

Fig. 13. Time evolution of the average Nusselt number at the heated wall for different inclinations.

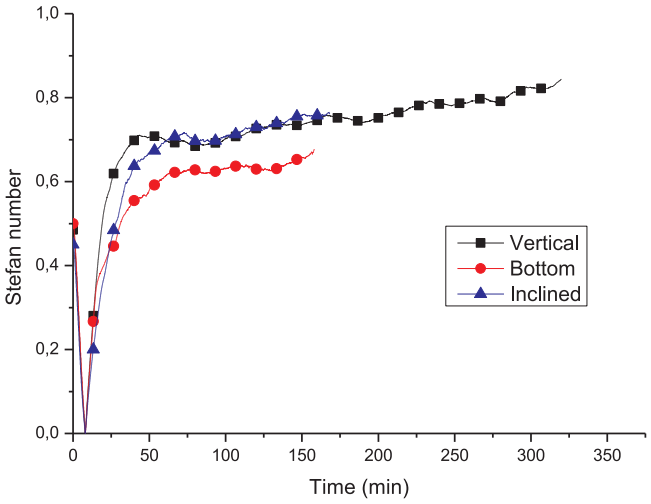

Fig. 14. Time evolution of the Stefan number for different inclinations.

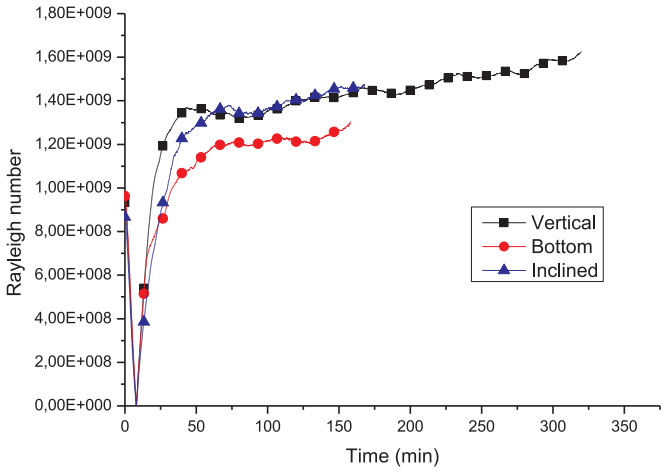

Fig. 15. Time evolution of the Rayleigh number at the heated wall for different inclinations.

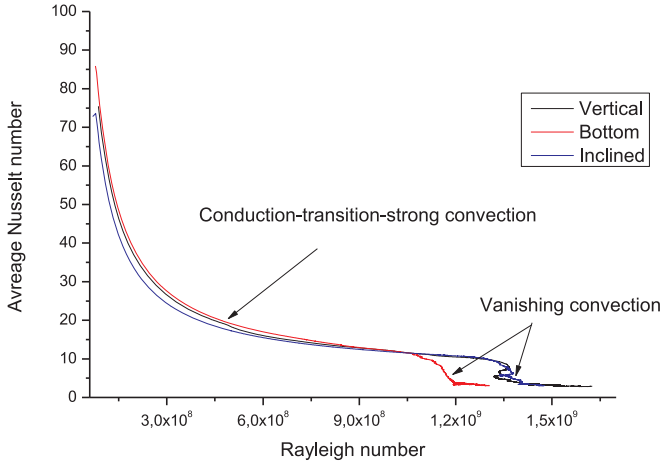

Fig. 16. Avreage Nusselt number as a function of the Rayleigh number.

90°: bottom) and time t (min). The liquid fraction evolution can be correlated mathematically by a following second-degree polynomial Eq. (1), with an average error of 7 % and a maximal error of 16 %, Fig. 8.

$$f_l(t) = (-10^{-9}\theta^2 + 3\times10^{-7}\theta - 7\times10^{-6})t^2 + (2\times10^{-7}\theta^2 - 3\times10^{-6}\theta - 0.0054)t \quad (1)$$

3.3. Temperature profiles

Fig. 9.a shows the time evolution of the temperature along the hot wall for the three inclinations. It observed that the temperature difference for the vertical case is always greater than the inclined case and to the bottom case. For the vertical case, the maximum temperature reaches about 78°C at $T(3,3)$ with a temperature difference of 49.5°C ($T(3,3)$ - $T(3,1)$), after 45 min. The maximum temperature becomes about 74°C with a temperature difference of 17°C, after 72 min. Thus, driven natural convection along the hot wall is more intense in the vertical case. In the bottom case, the temperature of the liquid close to the hot wall is fairly uniform. Fig. 9.b shows the time evolution of the temperature along the axis of the cavity perpendicular to the hot wall. It is observed that the temperature difference for the bottom case is principally greater than the inclined and vertical cases. For the bottom case, the maximum temperature reaches about 73°C at $T(3,2)$ with a temperature difference of 47°C ($T(3,2)$ - $T(1,2)$), after 66 min. The maximum temperature becomes 71 and 69°C with a temperature difference of 44 and 43°C after 87 min for the inclined and vertical cases, respectively. Thus, driven natural convection perpendicular to the hot wall is more intense in the case of the bottom. This explains the great intensity of natural convection and the acceleration of the melting rate in the bottom case.

3.4. Energy storage

The accumulative thermal energy stored within the paraffin is given by the Eq. 2.

$$Q_{st} = \sum_{t=t_i}^{t_s} [M_m C_s (T^{t+\Delta t} - T^t)] + \sum_{t=t_s}^{t_l} [M_m L_f f_l] + \sum_{t=t_l}^{t} [M_m C_l (T^{t+\Delta t} - T^t)] \quad (2)$$

Where Q_{st} (kJ) is the summed up of thermal energy stored by PCM from time $t = 0$, M_m (kg) the mass of PCM, C_s and C_l (kJ/kgK) the solid and liquid heat capacity of PCM, L_f (kJ/kg) latent heat of fusion of PCM, f_l liquid fraction of PCM, $T^{t+\Delta t}$ (°C) actual temperature of PCM and T^t (°C) is the previous temperature of PCM.

Fig. 10 shows the time evolution of the energy stored by PCM with different inclinations. At 60 min, the thermal energy stored reaches a value of about 53, 47 and 44 kJ by the paraffin in the bottom, inclined, and vertical hot wall cases, respectively. Thus, heating by bottom or 45° inclination can accelerate thermal energy stored by 20% and 7% compared to the vertical heating, respectively. After 120 min, the thermal energy stored reaches a value of 122, 106, and 88 kJ by the paraffin in the bottom, inclined and vertical cases. The thermal energy stored has increased by 39% and 21% for bottom and inclined cases compared to the vertical one. Thus, increasing the angle inclination leads to increasing the energy stored by paraffin.

The total heat loss from the enclosure can be calculated using the following Eq. 3:

$$Q_{loss} = \sum_{t=t_i}^{t} \left[M_{ins} C_{ins} (\bar{T}_{ins}^{t+\Delta t} - \bar{T}_{ins}^{t}) + \left(-K_{ins} S_{ins} \frac{\Delta T_{ins}}{\Delta x} \right) \Delta t \right] \quad (3)$$

Where Q_{loss} (kJ) is the summed up of thermal energy stored by insulation (Rockwool) and evacuated in the ambiance through the insulation. M_{ins}, C_{ins}, and K_{ins} are the mass, heat capacity, and thermal conductivity of Rockwool. $\bar{T}_{ins}^{t+\Delta t}$ is actual average temperature of insulation and $\bar{T}_{ins}^{t}$ is the previous average temperature one. Δx is the thickness of insulation (7.2 cm). Fig. 11 shows the time evolution of the energy loss by cavity with different inclinations. As it can be seen, heat loss from the enclosure is negligible in comparison with the energy stored. The total heat loss is less than 6% of the total energy stored at the end of the melting process in the bottom and inclined cases. However, the duration of the vertical case experiment leads to an increase in the heat loss that can reach 16.6% at the end of the melting process

3.5. Heat transfer characteristics

Fig. 12 shows time evolution of the heat flux transferred from the hot wall to the paraffin for different inclinations. The time evolution of the average Nusselt number at the heated wall are depicted in Fig. 13. The Nusselt number indicates the capacity of heat transfer in dimensionless form. Dimensionless average Nusselt number at hot side, based on the characteristic length of the cavity (height H) can be defined as Eq. 4.

$$Nu(t) = \frac{h(t) \times H}{K} \quad (4)$$

Where the surface-averaged natural convective heat transfer coefficient $h(t)$ is defined by Eq. 5.

$$h(t) = \frac{Q_{st}(t)}{A_w (T_w - T_m)\Delta t} \quad (5)$$

K is the thermal conductivity of paraffin, A_w the total surface area over which the heat flux is provided, T_w the average heated wall temperature and T_m the average melting temperature of the PCM (51.5°C).

For all inclination angles, the heat flux transferred to the paraffin increases rapidly to reach about 384, 404 and 413 W/m^2 for bottom, vertical and inclined cases after about 40 min. Thus, Nusselt numbers increases rapidly due to the rapid increase in temperature of the hot wall T_w.

As time progressed, the Nusselt numbers decrease over time until about 15min for bottom case and 20 min for vertical and inclined cases. This decrease can be correlated as Eq. 6.

$$Nu(t) = 10.68 + \frac{2417.47}{t - 500.11} \quad (6)$$

The initial large Nusselt numbers are attributed to the small thermal resistance of the very thin liquid layers at the start up time, which accordingly increases the heat transfer rates. With the disappearance of conduction, convection begins and its effect gradually dominates the heat transfer.When the melting of the paraffin starts, the liquid paraffin is still motionless and the heat transfer changes from conduction to convection (transition). Along with the development of liquid paraffin, the liquid begins to move due to the differences in density and the strong convection heat transfer begins to dominate the heat transfer. At the end, the vanishing convection regime develops until the total melting.

There are some differences in the duration of the strong convection for the three inclinations. Indeed, the heat flux decreases rapidly to stabilize around 134 W/m^2 after 70 min for bottom case and around 169 W/m^2 after 120 min for both vertical and inclined cases. The strong convection in the bottom case ends after 50 min and the global average Nusselt number during the strong convection is about 12.48. After, the Nusselt number decreases rapidly and becomes quasi-steady until the total melting. The strong convection ends after 56 and 60 min, and the Nusselt number becomes quasi-steady at 120 min for inclined and vertical cases, respectively. The global average Nusselt number during the strong convection is about 11.6 and 8.95 in the inclined and vertical cases. Thus, the strong convection is more intense in the bottom case and the global average Nusselt number increases during the strong convection by about 10% and 21% compared to the inclined and vertical cases.

The Stefan number of the melting process is defined as Eq. 7

$$Ste = \frac{C_l(T_w - T_m)}{L_f} \quad (7)$$

Fig. 14 shows time evolution of the Stefan number for different inclinations. Initially, the Stefan number decreases rapidly until the hot wall temperature exceeds the melting temperature T_m. Then, the Stefan number increases with the increase of the hot wall temperature and stabilizes around 0.77 ± 0.06, 0.65 ± 0.03 and 0.74 ± 0.02 for respectively vertical, bottom and inclined cases. In the steady stage, the average Stefan number reaches in this study around 0.72. The Stefan number affects the melting rate of the PCM. With the same PCM parameters, the change in the Stefan number reflects a change in the characteristic temperature difference. At low Stefan numbers, less time is consumed for melting. The increase of the Stefan number leads to a formation of complicated convective flow structures and an increase in the time for whole melting.

The Rayleigh number for the hot wall of the enclosure is defined in the usual way by Eq. 8

$$Ra = \frac{g\beta(T_w - T_m)H^3}{\nu\alpha} \quad (8)$$

Where g is the constant gravitational acceleration, β the coefficient of thermal expansion, ν the kinematic viscosity of the PCM liquid and α the thermal diffusivity of PCM.

Fig. 15 shows time evolution of the Rayleigh number at the heated wall for different inclinations. Initially, the Rayleigh number decreases rapidly until the hot wall temperature exceeds the melting temperature T_m. Then, the Rayleigh number increases with the increase of the hot wall temperature and stabilizes around an average value of respectively $1.12 \times 10^9 < 1.21 \times 10^9 < 1.3 \times 10^9$, $1.28 \times 10^9 < 1.39 \times 10^9 < 1.47 \times 10^9$ and $1.36 \times 10^9 < 1.45 \times 10^9 < 1.63 \times 10^9$ for all three cases bottom, inclined and vertical.

We investigate the relation between the heat flux represented by the average Nusselt number and the strength of buoyancy represented by the Rayleigh number in Fig. 16. We can see clearly that average Nusselt number decreases by power law with the increase of the Rayleigh number in the conduction, transition and the strong convection regimes. Indeed, Fig. 13 shows that Nu decreases globally during the melting of the paraffin when the strength of buoyancy becomes more important by the development of the liquid layer. In Fig. 16, conduction, transition and strong convection regimes are remarkably well distinguished depending on the range values of Nu defined by Fig. 13. In this regimes, the curves of Nu vs. Ra can be correlated by the following expression (Eq. 9) with a maximal error of 11 % and average error of 4 %:

$$\mathrm{Nu} = a(\mathrm{Ra})^b \quad (9)$$

	a	b
Vertical	4.72	-0.73
Bottom	7.97	-0.76
Inclined	1.84	-0.69

4. Conclusion

An experimental investigation was conducted to examine the effect of inclination angle on the thermal behavior of the melting process in a square enclosure heated from one side. The experimental study allowed drawing the following conclusions:

1 Initially, the melting process starts from the heated wall and the heat transfer is dominated by conduction. The intensity of heat transfer in the solid phase is lower than the liquid one due to the poor thermal conductivity of the paraffin. The heat transfer is characterized by the anticlockwise convection currents in the vertical case and Rayleigh-Benard multi cellular convection in the bottom case. In the inclined case, the heat flow begins with a Rayleigh-Benard multi cellular convection and then converts to the anticlockwise convection currents.

2 Paraffin melting is accompanied by a volumetric expansion around 7%. The study shows the creation of a concave shape on the free surface of the PCM at the end of each solidification caused by the volumetric shrinkage of paraffin. During melting, this phenomenon leads to the development of a cap form in the paraffin solid at the top of the melt layer. The length of this cap can reach around 23% and 55% of the width of free surface in the vertical and inclined cases. However, this phenomenon can be neglected in the bottom case. This phenomenon, which seriously disrupts the progression of melting, is generally neglected in numerical simulation work.

3 In the vertical case, the anticlockwise convection current developed in the liquid phase decreases the melting rate. Thus, the total melting time for the bottom and inclined cases were, on average, 56% and 48% less than the vertical case, respectively.

4 The thermal energy stored has increased by 39% and 21% for bottom and inclined cases compared to the vertical one. Thus, increasing the angle inclination leads to increasing the energy stored by paraffin.

5 Initially, Nusselt numbers increases rapidly due to the rapid increase of the hot wall temperature Tw. As time progressed, the Nusselt numbers decrease and conduction gradually disappears and changes to convection (transition). After, the liquid begins to move and strong convection dominates heat transfer and ends with vanishing convection until the total melting.

6 The strong convection is more intense in the bottom case and the global average Nusselt number increases during the strong convection by about 10% and 21% compared to the inclined and vertical cases.

Declaration of Competing Interest

The authors declare that they have no known competing financial interests or personal relationships that could have appeared to influence the work reported in this paper.

References

[1] R.K. Sharma, P. Ganesan, V.V. Tyagi, H.S.C. Metselaar, S.C. Sandaran, Developments in organic solid–liquid phase change materials and their applications in thermal energy storage, Energy Convers. Manag. 95 (2015) 193–228.
[2] N. Zhang, Y. Yuan, X. Cao, Y. Du, Z. Zhang, Y. Gui, Latent Heat Thermal Energy Storage Systems with Solid–Liquid Phase Change Materials: A Review, Adv. Eng. Mater. 20 (2018) 1700753.
[3] H. Guellil, A.N. Korti1, S. Abboudi, Experimental study of the performance of a novel latent heat charging unit on charging and discharging processes, J. Heat Mass Transf. 55 (2018) 855–866.
[4] A.N. Korti, F.Z. Tlemsani, Experimental investigation of latent heat storage in a coil in PCM storage unit, J. Energy Storage 5 (2016) 177–186.
[5] N.S. Bondareva, N.S. Gibanov, M.A. Sheremet, Computational Study of Heat Transfer inside Different PCMs Enhanced by Al2O3 Nanoparticles in a Copper Heat Sink at High Heat Loads, Nanomaterials 10 (2020) 284, https://doi.org/10.3390/nano10020284.
[6] S. Tiari, S. Qiu, Three-dimensional simulation of high temperature latent heat thermal energy storage system assisted by finned heat pipes, Energy Convers. Manag. 105 (2015) 260–271.
[7] A. Marušić, D. Lončar, Experimental validation of high-temperature latent heat storage model using melting front propagation data, Appl. Therm. Eng. 164 (2020) 114520.
[8] M. Fadl, P.C. Eames, A comparative study of the effect of varying wall heat flux on melting characteristics of phase change material RT44HC in rectangular test cells, Int. J. Heat Mass Transf. 141 (2019) 731–747.
[9] S. Madruga, J. Curbelo, Dynamic of plumes and scaling during the melting of a Phase Change Material heated from below, Int. J. Heat Mass Transf. 126 (2018) 206–220.
[10] W.-B. Ye, D.-S. Zhu, N. Wang, Effect of the inclination angles on thermal energy

storage in a quadrantal cavity, J. Therm. Anal. Calorim. 110 (2012) 1487–1492.
[11] H. Zennouhi, W. Benomar, T. Kousksou, A. Ait Msaad, A. Allouhic, M. Mahdaoui, T. El Rhafiki, Effect of inclination angle on the melting process of phase change material, Case Stud. Therm. Eng. 9 (2017) 47–54.
[12] Y. Hong, W.-B. Ye, S.-M. Huang, M. Yang, J. Du, Thermal storage characteristics for rectangular cavity with partially active walls, Int. J. Heat Mass Transf. 126 (2018) 683–702.
[13] N.S. Bondareva, B. Buonomo, O. Manca, M.A. Sheremet, Heat transfer performance of the finned nano-enhanced phase change, material system under the inclination influence, Int. J. Heat Mass Transf. 135 (2019) 1063–1072.
[14] B. Kamkari, H. Shokouhmand, F. Bruno, Experimental investigation of the effect of inclination angle on convection-driven melting of phase change material in a rectangular enclosure, Int. J. Heat Mass Transf. 72 (2014) 186–200.
[15] M.F. Bouadila, M.M. Oueslati, A. Guizani, A. Farhat, Enhancement of latent heat storage in a rectangular cavity: Solar water heater case study Salwa, Energy Convers. Manage. 78 (February 2014) 904–912.
[16] M.H. Joneidi, M.J. Hosseini, A.A. Ranjbar, R. Bahrampoury, Experimental investigation of phase change in a cavity for varying heat flux and inclination angles, Exp. Therm. Fluid Sci. 88 (2017) 594–607.
[17] M. Avci, M.Y. Yazici, An experimental study on effect of inclination angle on the performance of a PCM-based flat-type heat sink, Appl. Therm. Eng. 131 (2018) 806–814 25 February.
[18] X. Yang, Z. Guo, Y. Liu, L. Jin, Y.-L. He, Effect of inclination on the thermal response of composite phase change materials for thermal energy storage, Appl. Energy 238 (2019) 22–33.
[19] M.J. Allen, N. Sharifi, A. Faghri, T.L. Bergman, Effect of inclination angle during melting and solidification of a phase change material using a combined heat pipe-metal foam or foil configuration, Int. J. Heat Mass Transf. 80 (2015) 767–780.
[20] A. Agarwal, R.M. Sarviya, Characterization of Commercial Grade Paraffin wax as Latent Heat Storage material for Solar dryers, Mater Today Proceed. 4 (2017) 779–789.
[21] N. Ukrainczyk, S. Kurajica, J. Šipušiæ, Thermophysical Comparison of Five Commercial Paraffin Waxes as Latent Heat Storage Materials, Chem. Biochem. Eng. Q. 24 (2) (2010) 129–137.
[22] E. Assis, G. Ziskind, R. Letan, Numerical and Experimental Study of Solidification in a Spherical Shell, J. Heat Transf. 131 (2) (Feb 2009) 024502.